Acta Crystallographica Section A
Foundations of Crystallography
ISSN 0108-7673

Received 22 May 2007
Accepted 6 September 2007

The electron-spin–nuclear-spin interaction studied by polarized neutron scattering

Heinrich B. Stuhrmann

GKSS Forschungszentrum, Geesthacht, Germany, and Institut de Biologie Structurale Jean-Pierre Ebel, CEA/CNRS/UJF, F-38027 Grenoble, France. Correspondence e-mail: heinrich.stuhrmann@orange.fr

Dynamic nuclear spin polarization (DNP) is mediated by the dipolar interaction of paramagnetic centres with nuclear spins. This process is most likely to occur near paramagnetic centres at an angle close to 45° with respect to the direction of the external magnetic field. The resulting distribution of polarized nuclear spins leads to an anisotropy of the polarized neutron scattering pattern, even with randomly oriented radical molecules. The corresponding cross section of polarized coherent neutron scattering in terms of a multipole expansion is derived for radical molecules in solution. An application using data of time-resolved polarized neutron scattering from an organic chromium(V) molecule is tested.

1. Introduction

In a simple microscopic picture of dynamic nuclear spin polarization (DNP), the nuclear spin polarization develops near paramagnetic centres through the electron–nuclear dipolar interaction decreasing with the third power of the distance between electron and nuclear moments. More distant bulk nuclei are polarized by dipolar interaction between nuclei (spin diffusion). The same mechanism in reverse order is responsible for nuclear relaxation in most insulating solids.

In the frame of the solid effect (resolved or not) (Abragam & Goldman, 1978, 1982), the direct polarization of nuclear spins near paramagnetic centres is proportional to

$$W_{\text{solid effect}} \propto \left(\frac{\sin\theta\cos\theta}{r^3}\right)^2. \qquad (1)$$

From (1), it is clear that the direct polarization is a short-range effect which decreases rapidly with the distance r from the paramagnetic centre. Moreover, this effect is most pronounced at an angle of $\theta = 45°$ with respect to the direction of the external magnetic field **B** (Fig. 1).

To illustrate the probability of direct polarization, we refer to a chromium(V) complex, the sodium salt of bis(2-hydroxy-2-ethylbutyrato)oxochromate, $Na^+.(C_{12}H_{20}CrO_7)^-$, abbreviated as EHBA-$Cr^V$ (Krumpolc & Rožek, 1979). The wavefunction of its unpaired electron extends to a certain degree over the C atoms neighbouring the O atoms which surround the central Cr atom as is indicated by the dotted red lines in Fig. 1 (Wenckebach, 1980). The molecular structure shown in Fig. 1 has been given an orientation that is favourable for the polarization of its protons by the solid effect.

In a second step, the polarization of the nuclear spins will propagate to more distant nuclei by the interaction between nuclear spins. The probability of nuclear polarization by *flip-flop* is proportional to

$$W_{\text{flip-flop}} \propto \left(\frac{3\cos^2\theta - 1}{r^3}\right)^2. \qquad (2)$$

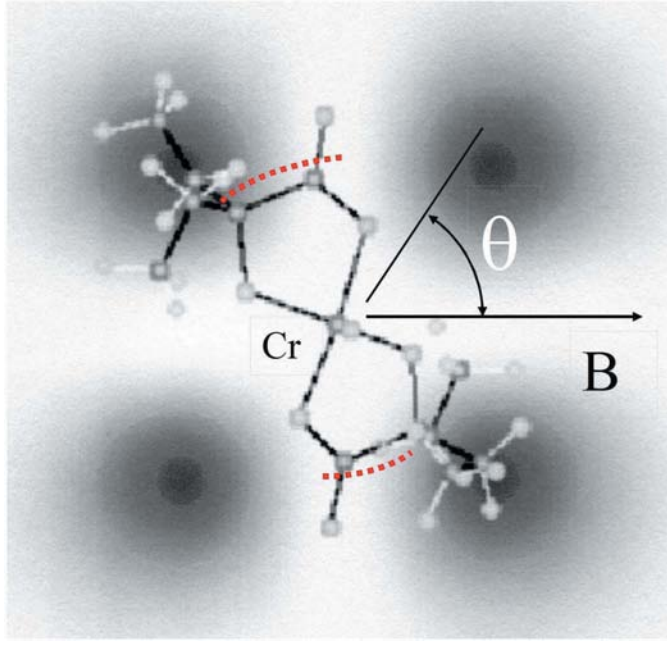

Figure 1
The probability W of the solid effect on proton spins of the EHBA-Cr^V molecule as described by equation (1). The interaction of the protons and the paramagnetic centre is that of separated point dipoles. The wavefunction of the unpaired electron extends to a certain degree over the C atoms (dotted lines). The oblique position of the EHBA-Cr^V molecule is favourable to the polarization of most of its protons by the solid effect.

Similar to the probability of the solid effect, the probability of flip-flop decreases rapidly with the distance between two nuclear spins. Contrary to what we have seen with the direct polarization, the propagation of the nuclear spin polarization proceeds preferentially along the direction of the external magnetic field and in the plane orthogonal to it.

Nuclear spin diffusion proceeds faster in regions with small magnetic field gradients, *i.e.* far away from paramagnetic centres. This is no longer the case for nuclear spins close to a paramagnetic centre, the so-called 'close nuclei'. The local magnetic field leads to a change of the Larmor frequency of each of the close nuclei which depends on their distance r from the paramagnetic centre and the angle θ with respect to the direction of the much stronger external magnetic field. In fact, the NMR profile of EHBA-Cr^V in a deuterated solvent consists of a broad peak due to close protons with relatively large deviations of their Larmor frequencies and a sharp peak due to protons with nearly equal Larmor frequencies (Fig. 2) (Niinikoski, 1980).

As the broad peak of NMR from EHBA-Cr^V is asymmetric, the interaction of these protons and the paramagnetic chromium cannot be entirely that of separated point dipoles (Cox, 1980).

The interplay between electron-spin–nuclear-spin interaction as given by (1) and the nuclear-spin diffusion as described by (2) will decide on the spatial distribution of polarized nuclear spins close to paramagnetic centres.

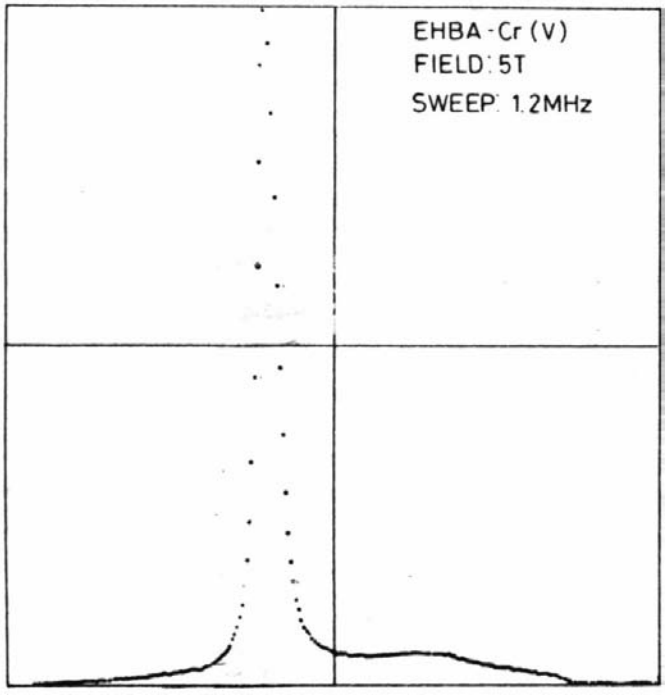

Figure 2
Proton NMR of EHBA-Cr^V dissolved in perdeuterated butanol (98% deuteration) and 5% by weight of heavy water. The narrow peak is interpreted as arising from the 2% of unsubstituted protons of the solvent. The broad line most likely comes from the protons belonging to the paramagnetic molecules dispersed rather uniformly in the solvent matrix (from Niinikoski, 1980). Copyright CERN.

Polarized neutron scattering is the method of choice to observe the build-up of proton polarization in space and time. Previous experiments on time-resolved neutron scattering from dynamically polarized protons of EHBA-Cr^V confirmed the special role of close protons. These experiments showed for the first time that the protons of EHBA-Cr^V are polarized to 20% within a second, whereas those of the deuterated solvent giving rise to a narrow peak of NMR (Fig. 2) were polarized much more slowly (van den Brandt *et al.*, 2002, 2003, 2006).

In the next step, a method will be presented which focuses on the interaction of the electron spin with the spins of the close protons. The non-spherical distribution of polarized protons near paramagnetic centres as predicted by (1) is expected to be imaged by the neutron scattering profile. In this paper, we give an estimate of the influence of direct polarization on the polarized neutron scattering intensity from radical molecules in solution.

2. The mathematical formalism

The scattering intensity $I(Q)$ of randomly oriented molecules in dilute solution is obtained as an average of intensities of coherent scattering,

$$I(Q) = \int_{\alpha=0}^{2\pi} \int_{\beta=0}^{\pi} \int_{\gamma=0}^{2\pi} |A(\mathbf{Q}, \alpha, \beta, \gamma)|^2 \, \mathrm{d}\alpha \sin\beta \, \mathrm{d}\beta \, \mathrm{d}\gamma. \quad (3)$$

$\mathbf{Q}$ is the scattering vector and $Q = |\mathbf{Q}| = (4\pi/\lambda)\sin\vartheta$ is its modulus (Fig. 3). 2ϑ is the scattering angle and λ is the wavelength. $A(\mathbf{Q}, \alpha, \beta, \gamma)$ is the scattering amplitude of the dissolved molecule after rotation by the Eulerian angles α, β, γ.

$$A(\mathbf{Q}, \alpha, \beta, \gamma) = \int_v \rho(\mathbf{Q}, \alpha, \beta, \gamma) \exp(i\mathbf{Q} \cdot \mathbf{r}) \, \mathrm{d}v. \quad (4)$$

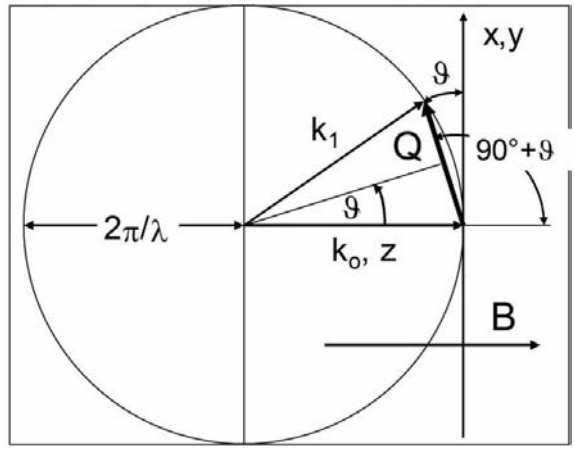

Figure 3
Scattering geometry. The scattering vector $\mathbf{Q}$ is the difference between the wavevector $\mathbf{k}_1$ and the wavevector $\mathbf{k}_0$ of the incident beam. The direction of the magnetic field $\mathbf{B}$ is shown to be along the direction z of the primary beam.

r is a vector in real space. $\rho(\mathbf{r}, \alpha, \beta, \gamma)$ is the scattering density of the dissolved molecule after rotation by (α, β, γ). The integration is performed over the molecular volume v.

In the presence of proton spins polarized by the solid effect, the average of the intensity given in (3) has to take into account the directional property of W in (1). It is therefore convenient to distinguish between the scattering density created by direct polarization and the scattering density which does not show directional properties, like those defined in (1).

The scattering amplitude due to direct polarization is

$$B(\mathbf{Q}, \alpha, \beta, \gamma) = \sum_j W_j(\alpha, \beta, \gamma) \exp[i\mathbf{Q} \cdot \mathbf{r}_j(\alpha, \beta, \gamma)]. \quad (5)$$

After rotation by (α, β, γ), the jth close proton at $\mathbf{r}_j = (x_j, y_j, z_j)$ finds itself at $\mathbf{r}_j(\alpha, \beta, \gamma) = \mathbf{r}'_j = (x'_j, y'_j, z'_j)$ and its probability $W_j \propto (\sin\theta_j \cos\theta_j)^2$ of direct polarization will change to $W_j \propto (\sin\theta'_j \cos\theta'_j)^2$, where $\cos\theta'_j = z'_j/r_j$. Here it has been assumed that the magnetic field direction coincides with the direction of the neutron beam.

If the direction of the magnetic field deviates from that of the neutron beam by an angle ε (Fig. 4), the probability of direct polarization of the jth proton has to be taken from W_j rotated by ε, *i.e.* by $W_j(\alpha, \beta, \gamma, \varepsilon)$. The scattering intensity $I(Q)$ is obtained by inserting the sum $A(\mathbf{Q}, \alpha, \beta, \gamma) + B(\mathbf{Q}, \alpha, \beta, \gamma, \varepsilon)$ in (3).

Both the expression for W and the integration over all orientations (α, β, γ) of the dissolved molecule suggest the use of polar coordinates and, more specifically, the development of the structure and of its amplitude as a series of spherical harmonics (§2.2). Before we enter into the general mathematical formalism, the origin of the asymmetry of the intensity distribution will be shown with a simpler case study.

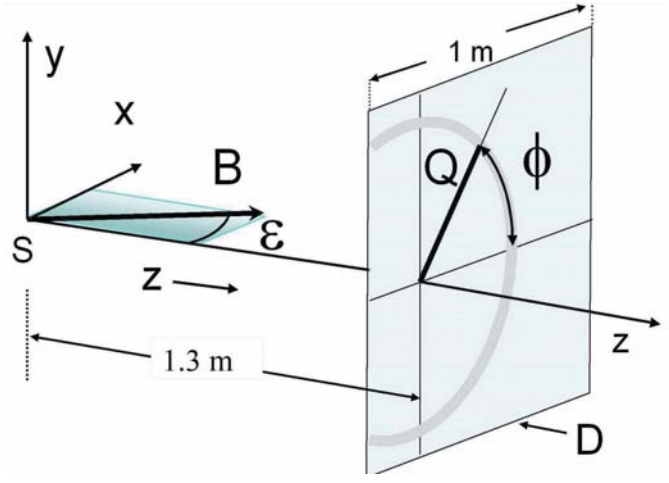

Figure 4
Scattering geometry. The direction of the neutron beam coincides with **z**. The direction of the external magnetic field (B) at the sample (S) differs from that of the neutron beam by ε. Right: the projection of the scattering vector (see Fig. 3) on the detector plane. The intensity of neutron scattering on the area detector (D) appears as a function of Q and ϕ.

2.1. An approximation for small ε

There are two reasons to discuss the expected asymmetry of polarized neutron scattering at small angles ε between the direction of the magnetic field and that of the neuron beam: firstly, this case is encountered with our experiments of time-resolved polarized neutron scattering from dynamically polarized proton spins (van de Brandt *et al.*, 2002, 2006) and, secondly, the asymmetry of polarized neutron scattering is described in relatively simple terms.

Two assumptions are made for an estimation of polarized neutron scattering from dynamically polarized protons of the EHBA-Cr^V molecule.

First, the protons of the ethyl groups at the two extremes of the molecule (Fig. 1) are represented by their centres of mass. For such a dumbbell object, the scattering amplitude (5) is written as

$$B(\mathbf{Q}, \alpha, \beta, \gamma, \varepsilon) = \sum_{j=1}^{2} W_j(\alpha, \beta, \gamma, \varepsilon) \exp(i\mathbf{Q} \cdot \mathbf{r}_j)(\alpha, \beta, \gamma). \quad (6)$$

On rotation by the Eulerian angles (α, β, γ), the centre of mass of the protons at $\mathbf{r}_1$ and $\mathbf{r}_2 = -\mathbf{r}_1$ of the EHBA-Cr^V molecule will be on a sphere with a radius $r = |\mathbf{r}_1| = |\mathbf{r}_2|$.

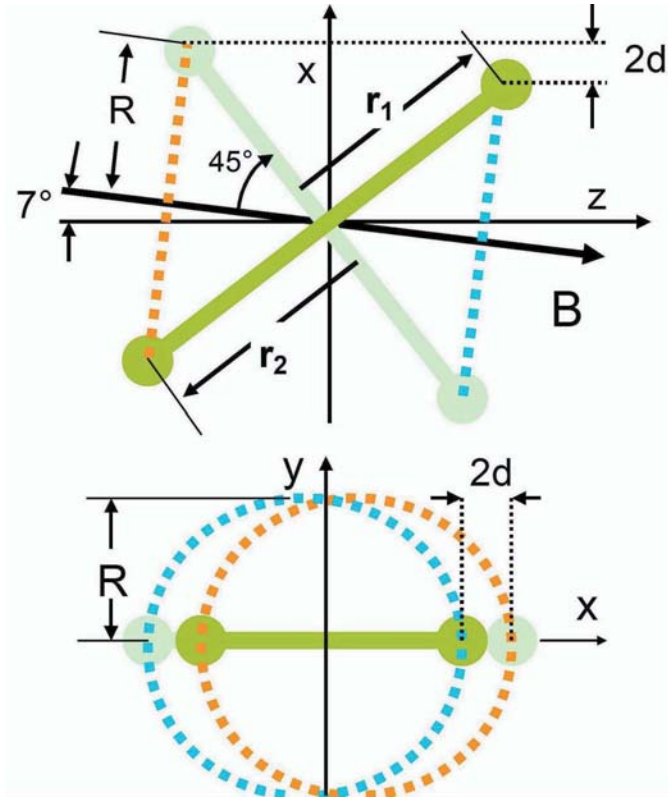

Figure 5
The spatial distribution of dumbbells [darker or lighter green spheres on dotted orange (blue) line], the orientations of which lie on the surface of a double cone with an opening angle of $\theta = \pm 45°$. The direction of the magnetic field **B** (= axis of double cone) differs from that of the neutron beam (z axis) by $\varepsilon = 7°$ (upper part). The two circles (dotted blue and orange) present the projection of the positions of the dumbbells (lower part).

The second assumption concerns the probability W of the electron-spin–proton-spin interaction, which will be restricted to the surface of a double cone with a total opening angle of 90°, *i.e.* to $\theta = 45°$ in (1). The axis of the double cone is that of the direction of the magnetic field at the sample. Dynamic proton spin polarization then takes place at the intersection of the double cone with the sphere of radius r, *i.e.* on two circles with the radius R centred at $z = R$ and $z = -R$, respectively (Fig. 5). For a magnetic field direction coinciding with that of the neutron beam, the two circles in the lower part of Fig. 5 would be indistinguishable.

As the direction of the magnetic field at the sample deviates from that of the neutron beam by ε, the two circles become displaced with respect to each other by $2d = 2R\varepsilon$ in the horizontal x direction (Fig. 5). The projection of the spatial distribution of the sites of DNP on the xy plane is asymmetric. Hence, an asymmetric profile of the intensity of polarized neutron small-angle scattering is expected. The width of the profile of small-angle scattering will be slightly narrower in the horizontal x direction. Using the Guinier approximation (see Appendix *A*), the difference between the intensities in horizontal and vertical directions is

$$\begin{aligned}\Delta I(Q) &= I(Q)_{\text{horizontal}} - I(Q)_{\text{vertical}} \\ &= \left(\exp\frac{-Q^2(R^2+d^2)}{2} + \exp\frac{-Q^2(R^2-d^2)}{2} \right. \\ &\quad \left. -2\exp\frac{Q^2R^2}{2}\right)\exp\frac{Q^2R_g^2}{6}. \end{aligned} \tag{7}$$

As the amplitude of dynamically polarized protons is usually much smaller than the amplitude of the atoms which are not subject to direct polarization [represented by $1/\exp(Q^2R_g^2/6)$], the dominant cross term is given (see Appendix *A*). The variation of the intensity difference $\Delta I(Q)$ with Q is shown in Fig. 12. The variation of the scattering intensity with the azimuth angle ϕ (Fig. 4) may be more complicated once larger ε and scattering angles 2ϑ are admitted. A detailed analysis of the intensity at constant Q as a function of ϕ then is mandatory.

2.2. Multipole expansion

The scattering amplitude $A(\mathbf{Q})$ is developed as a series of spherical harmonics $Y_{l,m}$ and spherical Bessel functions j_l [see equation (40)]:

$$\begin{aligned} A(\mathbf{Q}) &= \sum_j b_j \exp(i\mathbf{Q}\cdot\mathbf{r}_j) \\ &= \sum_{l=0}^{\infty}\sum_{m=-l}^{l} A_{l,m}(Q)Y_{l,m}(\Omega) \end{aligned} \tag{8}$$

with

$$A_{l,m}(Q) = (i)^l \sum_j b_j j_l(Qr_j)Y^*_{l,m}(\omega_j). \tag{9}$$

The components of the scattering factor $\mathbf{Q}$ in polar coordinates are Q, Ω, where Ω is a unit vector in the Fourier space (Fig. 3). The components of Ω giving rise to elastic coherent scattering are $\Theta = 90° + \vartheta$, ϕ (Figs. 3, 4). The position of the jth atom of the molecule is given by the polar coordinates r_j, θ_j, φ_j or r_j, ω_j, where ω_j is its unit vector in real space. The multipole expansion of the scattering amplitude $A(\mathbf{Q})$ provides an easy way to calculate the scattering function $I(\mathbf{Q})$ of randomly oriented particles in solution.

$$I(Q) = \int |A(\mathbf{Q})|^2 \,\mathrm{d}\Omega \propto \sum_{l=0}^{\infty}\sum_{m=-l}^{l} |A_{l,m}(Q)|^2. \tag{10}$$

This formula not only gives an easy access to the symmetry of isomeric viruses (Finch & Holmes, 1967) but it also provides the set of structures giving rise to the same scattering function $I(Q)$ (Stuhrmann, 1970).

The electron-spin–proton-spin interaction will lead to a polarization of the protons close to the paramagnetic centres as is described by (1) (Fig. 1). Substituting the scattering length b_j in (9) by the probability W_j as defined by (1), one obtains

$$\begin{aligned} &B(\mathbf{Q}, \alpha, \beta, \gamma, \varepsilon) \\ &\quad = \sum_{l=0}^{\infty}(i)^l \sum_{m=-l}^{l}\sum_j W_j(\alpha,\beta,\gamma,\varepsilon) j_l(Qr_j) Y^*_{l,m}(\omega'_j) Y_{l,m}(\Omega) \\ &\quad \equiv \sum_{l=0}^{\infty}\sum_{m=-l}^{l} B_{l,m}(Q,\alpha,\beta,\gamma,\varepsilon) Y_{l,m}(\Omega), \end{aligned} \tag{11}$$

where ω'_j is the unit vector pointing to the jth atom after rotation by α, β, γ. The averaged scattering intensity from polarized protons near paramagnetic centres is then

$$I_{BB}(\mathbf{Q},\varepsilon) = \int_{\alpha=0}^{2\pi}\int_{\beta=0}^{\pi}\int_{\gamma=0}^{2\pi} |B(\mathbf{Q},\alpha,\beta,\gamma,\varepsilon)|^2 \,\mathrm{d}\alpha \sin\beta \,\mathrm{d}\beta \,\mathrm{d}\gamma. \tag{12}$$

There are various ways to calculate the integrand in (12) and to perform the integration. All of them result in an expansion of the scattered intensity in terms of spherical harmonics with both l and m being even.

$$I_{BB}(\mathbf{Q},\varepsilon) = \sum_{l=0}^{\infty}\sum_{m=-l}^{l} I_{l,m}(Q,\varepsilon) Y_{l,m}(\Omega). \tag{13}$$

Owing to the presence of $I_{l,m}(Q)$ with $l > 0$ and $|m| > 0$, the scattering intensity $I_{BB}(\mathbf{Q}, \varepsilon)$ will be non-spherical.

2.2.1. Numerical integration. In a first step, the atomic coordinates (x_j, y_j, z_j) of the jth proton of the solute molecule are rotated by the Eulerian angles (α, β, γ). The amplitude is calculated from the rotated coordinates (x'_j, y'_j, z'_j) by using (9).

In a second step, the atoms at (x'_j, y'_j, z'_j) are rotated by ε. The probability of direct polarization W is obtained from the coordinates (x''_j, y''_j, z''_j), which have been rotated by ε.

$$W_j(\alpha,\beta,\gamma,\varepsilon) = \left(\frac{z''_j}{r_j}\right)^2\left(1-\frac{z''_j}{r_j}\right)^2. \tag{14}$$

The variation of W in (1) with the distance r of different close protons from the paramagnetic centre is neglected. Such an approximation may hold for relatively small organic radicals, like the EHBA-Cr^V molecule, where the H atoms are at distances between 3 and 5 Å from the central Cr atom (Fig. 1).

The expression of intensity $|B(\mathbf{Q},\alpha,\beta,\gamma,\varepsilon)|^2$ in (12) contains products of spherical harmonics that are reduced to sums of these by using (42) and (43).

$$\begin{aligned}
&B_{l_1,m_1}(Q,\ldots)B^*_{l_2,m_2}(Q,\ldots)Y_{l_1,m_1}(\Omega)Y^*_{l_2,m_2}(\Omega)\\
&\quad=\sum_{l=|l_1-l_2|}^{l_1+l_2}\sum_{m=-l}^{l}(-1)^{m+m_2}\left[\frac{(2l_1+1)(2l_2+1)(2l+1)}{4\pi}\right]^{1/2}\\
&\qquad\times\begin{pmatrix}l_1 & l_2 & l\\ 0 & 0 & 0\end{pmatrix}\begin{pmatrix}l_1 & l_2 & l\\ m_1 & -m_2 & m\end{pmatrix}\\
&\qquad\times B_{l_1,m_1}(Q,\ldots)B^*_{l_2,m_2}(Q,\ldots)Y_{l,-m}(\Omega)\\
&\qquad\Rightarrow S_{l,-m}(Q,\alpha,\beta,\gamma,\varepsilon)Y_{l,-m}(\Omega). \qquad (15)
\end{aligned}$$

The arrow in (15) means 'contributes to'. The integration over all orientations of the structure results in an anisotropic distribution of the scattering intensity:

$$\begin{aligned}
I_{BB}(\mathbf{Q},\varepsilon)&=\sum_{l=0}^{\infty}\sum_{m=-l}^{l}Y_{l,m}(\Omega)\\
&\quad\times\int_{\alpha=0}^{2\pi}\int_{\beta=0}^{\pi}\int_{\gamma=0}^{2\pi}S_{l,m}(Q,\alpha,\beta,\gamma,\varepsilon)\,\mathrm{d}\alpha\sin\beta\,\mathrm{d}\beta\,\mathrm{d}\gamma\\
&=\sum_{l=0}^{\infty}\sum_{m=-l}^{l}I_{l,m}(Q,\varepsilon)Y_{l,m}(\Omega). \qquad (16)
\end{aligned}$$

2.2.2. The analytical expression. There is a way to avoid the numerical integration in (16) by using mathematical tools which have proven to be useful in quantum mechanics of angular momentum. Some of the relevant formula are given in Appendix *C*.

The analytical expression is derived in Appendix *B*. Here we just give a brief outline.

The angular part of the probability function W in (1) is expressed by spherical harmonics.

$$W(\theta)=|Y_{2,1}(\theta,\varphi)|^2=\sum_{k=0,2,4}C_kY_{k,0}(\theta). \qquad (17)$$

The coefficients C_k are obtained by using (42) and (43): C_0 = 0.47266, C_2 = 0.15098, C_4 = −0.27009.

The amplitude $B(\mathbf{Q},\alpha,\beta,\gamma)$ in (11) is now completely described by expansions as series of spherical harmonics.

The rotation of the spherical harmonics by (α,β,γ)

$$Y^*_{l,m}(\omega'_j)=\sum_{m'=-l}^{l}R_{l,m',m}(\alpha,\beta,\gamma)Y^*_{l,m'}(\omega_j) \qquad (18)$$

enters the matrix elements $R_{l,m',m}(\alpha,\beta,\gamma)$. Their orthogonality relation

$$\begin{aligned}
&\frac{1}{8\pi^2}\int_{\alpha=0}^{2\pi}\int_{\beta=0}^{\pi}\int_{\gamma=0}^{2\pi}R_{l_1,m'_1,m_1}(\alpha,\beta,\gamma)R^*_{l_2,m'_2,m_2}(\alpha,\beta,\gamma)\,\mathrm{d}\alpha\sin\beta\,\mathrm{d}\beta\,\mathrm{d}\gamma\\
&\quad=\frac{1}{2l+1}\delta_{l_1,l_2}\delta_{m'_1,m'_2}\delta_{m_1,m_2} \qquad (19)
\end{aligned}$$

provides an elegant solution of the integral in (12).

$$\begin{aligned}
&I_{BB}(\mathbf{Q},\varepsilon)\\
&\quad=\sum_{l_1=0}^{\infty}\sum_{l_2=0}^{\infty}i^{l_1}(-i)^{l_2}\sum_{l=|l_1-l_2|}^{l_1+l_2}\sum_{m=-l}^{l}\sum_{m_1=-l_1}^{l_1}\sum_{m_2=-l_2}^{l_2}(-1)^{m+m_2}\\
&\qquad\times\left[\frac{(2l_1+1)(2l_2+1)(2l+1)}{4\pi}\right]^{1/2}\begin{pmatrix}l_1 & l_2 & l\\ m_1 & -m_2 & m\end{pmatrix}\\
&\qquad\times\begin{pmatrix}l_1 & l_2 & l\\ 0 & 0 & 0\end{pmatrix}\sum_{k_1=0,2,4}\sum_{k_2=0,2,4}\frac{4\pi C_{k_1}C_{k_2}}{[(2k_1+1)(2k_2+1)]^{1/2}}\\
&\qquad\times\sum_{n_1=-k_1}^{k_1}\sum_{n_2=-k_2}^{k_2}Y^*_{k_1,n_1}(\varepsilon_2,\varepsilon_1)Y_{k_2,n_2}(\varepsilon_2,\varepsilon_1)\sum_{\eta}(2\eta+1)\\
&\qquad\times\sum_{n'_1=-k_1}^{k_1}\sum_{n'_2=-k_2}^{k_2}\sum_{m'_1=-l_1}^{l_1}\sum_{m'_2=-l_2}^{l_2}\begin{pmatrix}l_1 & k_1 & \eta\\ m'_1 & n'_1 & p\end{pmatrix}\begin{pmatrix}l_1 & k_1 & \eta\\ m_1 & n_1 & q\end{pmatrix}\\
&\qquad\times\begin{pmatrix}l_2 & k_2 & \eta\\ m'_2 & n'_2 & p\end{pmatrix}\begin{pmatrix}l_2 & k_2 & \eta\\ m_2 & n_2 & q\end{pmatrix}\\
&\qquad\times\sum_{j_1}\sum_{j_2}Y^*_{k_1,n'_1}(\omega_{j_1})Y_{k_2,n'_2}(\omega_{j_2})j_{l_1}(Qr_{j_1})j_{l_2}(Qr_{j_2})Y^*_{l_1,m'_1}(\omega_{j_1})\\
&\qquad\times Y_{l_2,m'_2}(\omega_{j_2})Y_{l,-m}(\Omega). \qquad (20)
\end{aligned}$$

For η two conditions hold: $|l_1-k_1|\le\eta\le l_1+k_1$ and $|l_2-k_2|\le\eta\le l_2+k_2$.

In many applications, the cross term

$$\begin{aligned}
I_{AB}(\mathbf{Q},\varepsilon)&=\int_{\alpha=0}^{2\pi}\int_{\beta=0}^{\pi}\int_{\gamma=0}^{2\pi}\mathrm{d}\alpha\sin\beta\,\mathrm{d}\beta\,\mathrm{d}\gamma\\
&\quad\times\mathrm{Re}\{A(\mathbf{Q},\alpha,\beta,\gamma)B^*(\mathbf{Q},\alpha,\beta,\gamma,\varepsilon)\} \qquad (21)
\end{aligned}$$

may be more important than the term depending on the amplitude of the polarized spins only, a point which is addressed in (31). One way to obtain the cross term $I_{AB}(\mathbf{Q},\varepsilon)$ from (20) is to restrict the sum over k_1 (or k_2) to its first member.

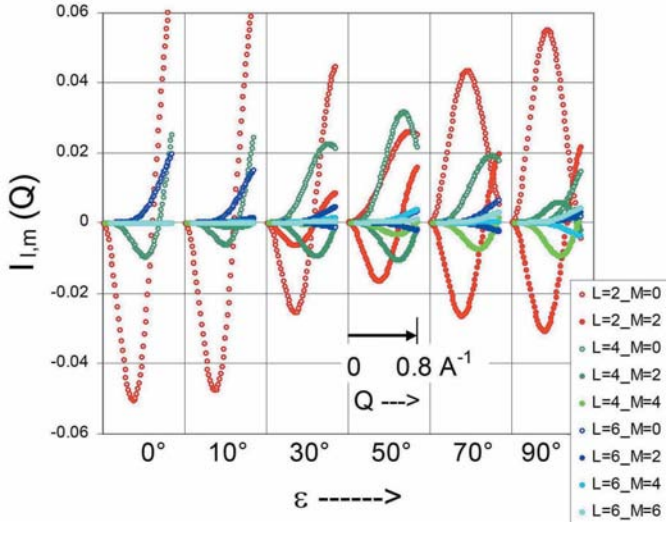

Figure 6
The radial functions $I_{l,m}(Q,\varepsilon)$ of the intensity of polarized neutron scattering from a clover-leaf distribution of polarized protons near the paramagnetic centres of EHBA-Cr^{V}. At ε = 0, components with $m\neq 0$ vanish. The functions are normalized to $I_{0,0}(0)$ = 1.

3. Results and discussion

As already mentioned in the *Introduction*, EHBA-Cr^V dissolved in a mixture of deuterated glycerol and D_2O has been chosen to illustrate the anisotropy of polarized neutron scattering from dynamically polarized proton spins. The following calculation is based on the assumption that the clover-leaf distribution of the proton polarization near the paramagnetic centre shown in Fig. 1 is maintained to a good extent for some time, typically for 1 s, after the onset of DNP. Within this time, the propagation of nuclear polarization by dipolar interaction between nuclear spins is assumed to be negligible. The corresponding functions $I_{l,m}(Q,\varepsilon)$ as defined by (16) are shown in Fig. 6 for various angles ε.

The intensity (16) involves the multiplication of the radial functions $I_{l,m}(Q,\varepsilon)$ with the corresponding $Y_{l,m}(\Omega)$. Fig. 7 shows $I(\mathbf{Q},\varepsilon=90^\circ)$ diminished by the average intensity $I(Q,\varepsilon=90^\circ)$, *i.e.* the multipoles of $I(\mathbf{Q},\varepsilon=90^\circ)$ with $|m|>0$. It is this kind of intensity pattern that one would expect to see on an area counter after subtraction of the spherical average intensity.

Fig. 8 shows the same $I(\mathbf{Q},\varepsilon)$ for some Q and ε as a function of the angle ϕ (for ϕ see Fig. 4). There is no variation of the intensity for $\varepsilon = 0$, *i.e.* when the direction of the magnetic field at the sample coincides with the direction of the neutron beam. The variation of the intensity with ϕ increases with ε, and for larger Q the contribution of higher multipoles ($l \geq 4$) is more pronounced.

In the next step, we assume that there is an important interaction between nuclear spins leading to a uniform polarization of the protons of the EHBA-Cr^V molecule in a very short time. The variation of the intensity with ϕ shown in Fig. 9 then is somewhat weaker than that we have seen before. As there are hardly any protons in the deuterated solvent, the dipolar interaction between protons as described by (2) is restricted to those of the EHBA-Cr^V molecule. It is the spatial arrangement of the protons in two domains, like a dumb bell, which leads to a selection of the EHBA-Cr^V molecules for DNP according to their orientation with respect to the direction of the external magnetic field (Fig. 1). The scattering intensity $I(\mathbf{Q},\ \varepsilon = 0)$ differs from $I(Q)$ using the Debye equation of X-ray scattering from gas molecules, denoted by D in Figs. 8 and 9.

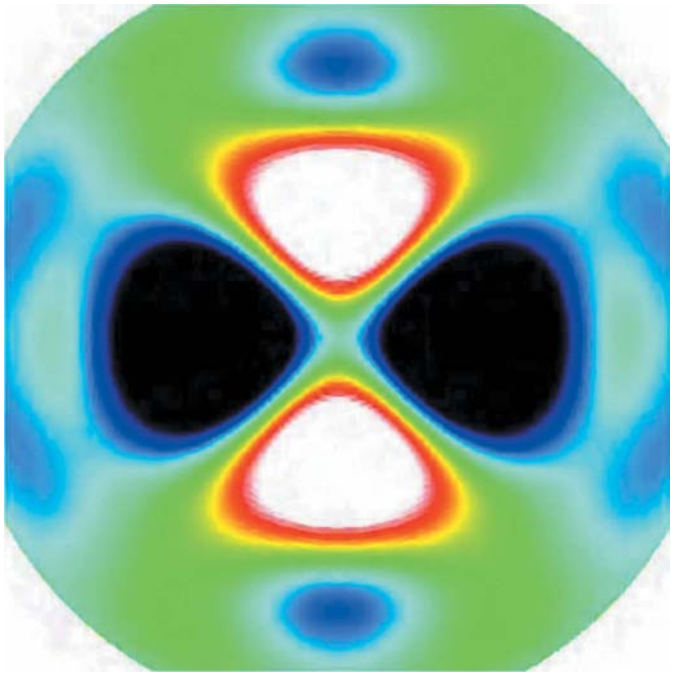

Figure 7
The asymmetric intensity distribution on the area detector. The magnetic field direction is orthogonal to the direction of the neutron beam (ε = 90°). The multipole components that do not give rise to a variation of the intensity with ϕ, *i.e.* those with m = 0, have been removed.

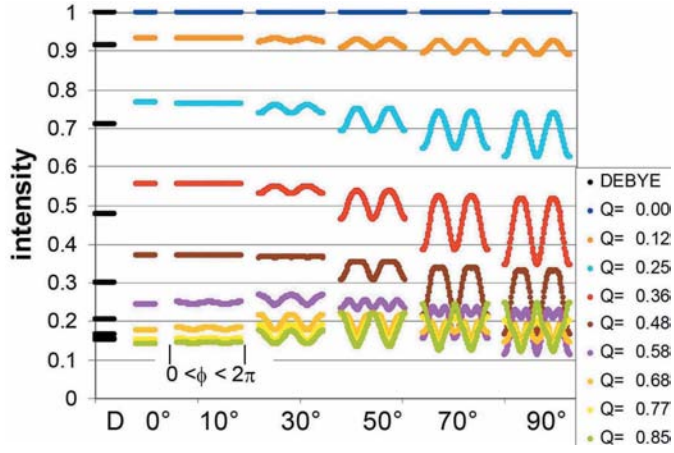

Figure 8
The variation of the scattering intensity $I_{BB}(\mathbf{Q},\varepsilon)$ from the 20 protons of EHBA-Cr^V with the azimuth ϕ in the detector plane at various Q (Å^{-1}) and various angles ε in the absence of dipolar interaction between proton spins. The left column (black bars, denoted by D) presents the scattering of the 20 protons of EHBA-Cr^V using (10).

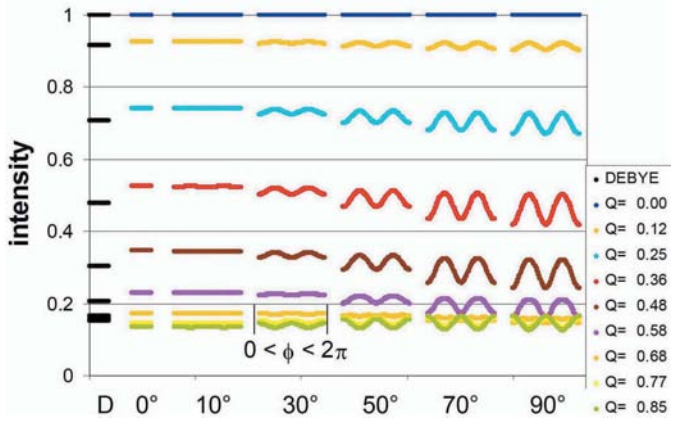

Figure 9
The variation of the scattering intensity $I_{BB}(\mathbf{Q},\varepsilon)$ from the 20 protons of EHBA-Cr^V with the azimuth ϕ in the detector plane at various Q (Å^{-1}) and various angles ε. There is dipolar interaction between proton spins leading to a uniform polarization of the 20 protons of the molecule. The left column (black bars, denoted by D) presents the scattering of the 20 protons of EHBA-Cr^V using (10).

So far, the calculation of the intensity started from the H atoms of the EHBA-Cr^V molecule only. Including the non-H atoms of the EHBA-Cr^V molecule and taking into account its contrast in a deuterated solvent, the resulting amplitude $A(\mathbf{Q})$ is much larger than that of the polarized protons. The polarization-dependent intensity is largely due to the cross terms $I_{AB}(\mathbf{Q}, \varepsilon)$ as defined by (21). Figs. 10 and 11 show the cross term of the intensity without and with dipolar interaction between proton spins, respectively. The variation of the intensity with ϕ is slightly smaller than with the corresponding scattering functions with protons only. Even with a very frequent dipolar interaction between proton spins leading to an average polarization among the 20 protons of an EHBA-Cr^V molecule, the asymmetry of the intensity distribution is strong enough to be measurable at reasonably large ε (Fig. 11).

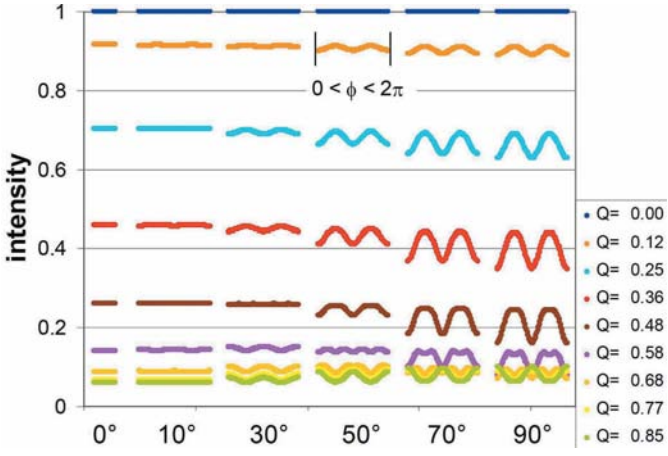

Figure 10
The variation of the scattering intensity $I_{AB}(\mathbf{Q}, \varepsilon)$ of EHBA-Cr^V with the azimuth ϕ in the detector plane at various Q (Å^{-1}) and various angles ε in the absence of dipolar interaction between proton spins.

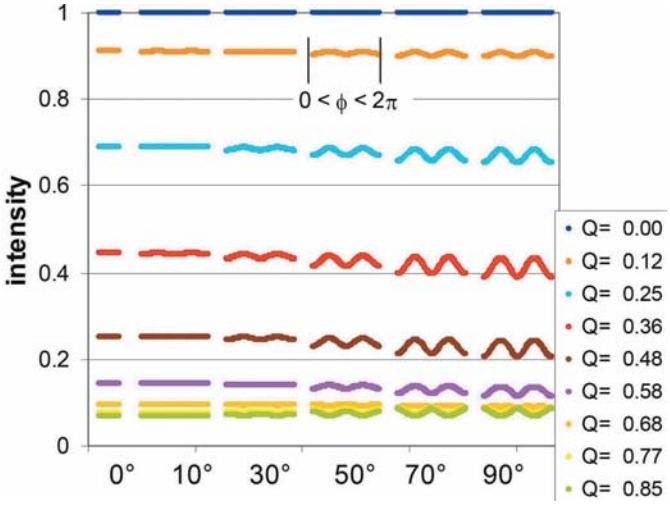

Figure 11
The variation of the scattering intensity $I_{AB}(\mathbf{Q}, \varepsilon)$ with the azimuth ϕ in the detector plane at various Q (Å^{-1}) and various angles ε with important dipolar interaction between proton spins leading to a uniform polarization of the 20 protons in each EHBA-Cr^V molecule.

The experiments of time-resolved polarized neutron scattering from EHBA-Cr^V at the instrument D22 of the Institut Laue–Langevin (ILL), Grenoble, France, happened to be performed with $\varepsilon = 7^\circ$ in the horizontal plane (van den Brandt *et al.*, 2002). As the EHBA-Cr^V molecule with a radius of gyration R_g = 3.5 Å is a relatively small molecule, a large Q range was required to measure the central peak of polarized neutron scattering. The detector was moved to an asymmetric position and the axis of the solenoid was tilted by $\varepsilon = 7^\circ$ (Fig. 4).

The expected variation of the intensity with ϕ is then very small, less than 0.001 of the polarization-dependent intensity at $Q = 0$ (Fig. 12). As the direction of DNP was inverted each 10 s, the change of the asymmetry during one cycle of positive and negative DNP could be extracted from many hundreds of sequences of 200 pictures with a remarkably good accuracy of about ±0.1%. The experimental result given as the difference between the intensity in the horizontal direction and that of the vertical direction on the area detector agrees with the calculated scattering curves within the statistical error (Fig. 12). The accuracy of the experimental data is not good enough to discriminate between different models. For instance, it cannot be decided whether the dipolar interaction between proton spins leads to a uniform polarization of the protons in each molecule.

4. Conclusions

The clover-leaf-like probability function (1) of electron-spin–proton-spin interaction or direct nuclear polarization is the origin of a non-spherical distribution of the intensity of polarized neutron scattering from radical molecules in

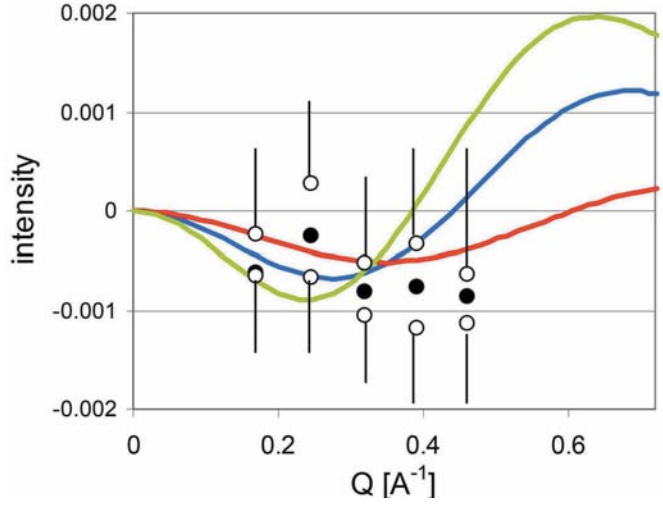

Figure 12
The asymmetry of neutron scattering from directly polarized protons of EHBA-Cr^V. Experimental data are given by circles. The open circles result from a tentative shift of the origin of the primary beam by 3 mm in either the left or the right direction on the area counter (Fig. 4). Corresponding calculated scattering of the EHBA-Cr^V model: without dipolar interaction between polarized protons (blue), with dipolar interaction between protons (red), Guinier approximation (green) [equation (31)].

solution. This type of scattering pattern is even enhanced when the probability function of direct polarization selects almost rod-like molecules according to their orientation in solution with respect to the direction of an external magnetic field, as is the case for the EHBA-Cr^V molecule. An eventually important dipolar interaction between protons close to the paramagnetic centre then decreases the variation of the intensity of polarized neutron scattering at constant Q to some extent, in particular at higher structural resolution, *i.e.* at higher Q.

The experimental data, which were obtained with a rather small ε of only 7°, indicate a variation of the intensity of less than 0.1%, in agreement with the calculated functions but too small to discriminate between different models.

A much larger variation of the intensity at constant Q is expected with an increased ε. A more appropriate choice of an angle, say $\varepsilon = 40°$, which is perfectly feasible with the polarized target facility of the Paul-Scherrer-Institut (van den Brandt *et al.*, 2002), would reveal a more detailed microscopic picture of the electron-spin–proton-spin interaction and of the dipolar interaction between proton spins. From the variation of the intensity of polarized neutron scattering with the angle ϕ as a function of Q, the range of direct polarization and the transition to nuclear spin diffusion can be obtained. The influence of the magnetic spin diffusion barrier (Hayter *et al.*, 1974; Cox *et al.*, 1977) on the build-up of nuclear polarization in space and time could be clarified by time-resolved polarized neutron scattering.

APPENDIX *A*
Approximation for small ε

At small scattering angles, the z component of the scattering vector $\mathbf{Q}$ can be neglected (Fig. 3).

$$B(\mathbf{Q}) = \sum_{j=1}^{2} W_j \exp[i(x_j Q_x + y_j Q_y)]. \tag{22}$$

Starting from the two assumptions made in §2.1, and setting $W = 1$, the amplitude in the vertical y direction (Fig. 5), $B_V(Q)$, is given by

$$B_V(Q) = \sum_{j=1}^{4} \exp(iy_j Q) = \sum_{j=1}^{4} \cos(y_j Q) + i \sin(y_j Q). \tag{23}$$

The index runs over the positive and negative values of both circles defined in §2.1. With $y_2 = -y_1$, $y_4 = -y_3$ of the two circles shown in Fig. 5 and $|y_j| = R$, $j = 1, 2, 3, 4$ (Fig. 5), one obtains

$$B_V(Q) = 4\cos(RQ). \tag{24}$$

For the horizontal x direction, the projection of the lengths of the two dumbbells require $x_1 = R - d$, $x_2 = -R + d$ (green in Fig. 5), $x_3 = R + d$, $x_4 = -R - d$ (light green in Fig. 5) and $|x_j| = R$, $j = 1, 2, 3, 4$. The corresponding amplitude $B_H(Q)$ is given by

$$B_H(Q) = 2\cos[(R + d)Q] + 2\cos[(R - d)Q]. \tag{25}$$

The cosines in (24) and (25) are replaced by their expansions as power series of Q^2.

$$B_V(Q) = 2(1 - \tfrac{1}{2}R^2Q^2 + \ldots - \ldots) \tag{26}$$

$$B_H(Q) = 2[1 - \tfrac{1}{2}(R + d)^2Q^2 + \ldots - \ldots) + 2[1 - \tfrac{1}{2}(R - d)^2Q^2 + \ldots - \ldots]. \tag{27}$$

Using the Guinier approximation, one obtains

$$B_V(Q) = 4\exp[-\tfrac{1}{2}R^2Q^2] \tag{28}$$

$$B_H(Q) = 2\exp[-\tfrac{1}{2}(R + d)^2Q^2] + 2\exp[-\tfrac{1}{2}(R - d)^2Q^2]. \tag{29}$$

The amplitude of the atoms of the EHBA-Cr^V molecule that are not subject to DNP is given by

$$A(Q) = \exp(-\tfrac{1}{6}R_q^2Q^2). \tag{30}$$

R_g is the corresponding radius of gyration.

The difference between the intensity in the horizontal x direction and that in the vertical y direction is

$$\begin{aligned}\Delta I(Q) &= I_H(Q) - I_V(Q)\\ &= |A(Q) + B_H(Q)|^2 - |A(Q) + B_V(Q)|^2\\ &\approx \mathrm{Re}\{[B_H(Q) - B_V(Q)]A(Q)\}\\ &= \left(\tfrac{1}{2}\exp\frac{-Q^2(R^2 + d^2)}{2} + \tfrac{1}{2}\exp\frac{-Q^2(R^2 - d^2)}{2} - \exp\frac{Q^2R^2}{2}\right)\exp-\frac{Q^2R_g^2}{6}.\end{aligned} \tag{31}$$

As the amplitudes $B_H(Q)$ and $B_V(Q)$ are much smaller than $A(Q)$, the absolute squares of B in (31) have been omitted.

APPENDIX *B*
The analytical expression

We start from the scattering amplitude $B(\mathbf{Q}, \alpha, \beta, \gamma, \varepsilon)$ as defined by (11). While an explicit expression for $Y_{l,m}(\omega_j')$ has been given in (18), (17) presents the probability function W in its standard form, *i.e.* with the direction of the magnetic field along the z axis (the direction of the neutron beam). What is the strength of W at the site of the jth atom after rotation of the molecule by the Eulerian angles α, β, γ in a magnetic field the direction of which is deviating from that of the neutron beam by the Eulerian angles ε_1, ε_2, ε_3?

In the first step, $W(\theta)$ as defined by (17) is rotated by ε_1, ε_2, ε_3. Using (44), one obtains

$$W(\omega) = \sum_{k=0,2,4} C_k \sum_{n=-k}^{k} R_{k,n,0}(\varepsilon_1, \varepsilon_2, \varepsilon_3) Y_{k,n}(\omega). \tag{32}$$

According to (45), the matrix elements $R_{k,n,0}$ can be expressed by spherical harmonics $Y_{k,n}$.

$$W(\omega) = \sum_{k=0,2,4} C_k \left[\frac{4\pi}{2k + 1}\right]^{1/2} \sum_{n=-k}^{k} Y_{k,n}^*(\varepsilon_2, \varepsilon_1) Y_{k,n}(\omega). \tag{33}$$

This is the probability of direct polarization in a magnetic field which has been rotated by ε_1, ε_2 with respect to the direction of the neutron beam.

In the next step, we would like to know $W(\omega_j')$ of the jth proton which has been rotated by (α, β, γ), *i.e.*

$$W(\omega_j') = \sum_{k=0,2,4} C_k \left[\frac{4\pi}{2k+1}\right]^{1/2} \sum_{n=-k}^{k} Y_{k,n}^*(\varepsilon_2, \varepsilon_1) Y_{k,n}(\omega_j'). \quad (34)$$

Using (44), one obtains

$$W_j(\alpha, \beta, \gamma, \varepsilon) = \sum_{k=0,2,4} C_k \left[\frac{4\pi}{2k+1}\right]^{1/2} \sum_{n=-k}^{k} Y_{k,n}^*(\varepsilon_2, \varepsilon_1) \times \sum_{n'=-k}^{k} R_{k,n',n}(\alpha, \beta, \gamma) Y_{k,n'}(\omega_j). \quad (35)$$

Inserting (18) and (35) in (11), one obtains the explicit expression for $B_{l,m}(Q, \alpha, \beta, \gamma, \varepsilon)$.

$$\begin{aligned} B_{l,m}(Q, \alpha, \beta, \gamma, \varepsilon) &= (i)^l \sum_j \sum_{k=0,2,4} C_k \left[\frac{4\pi}{2k+1}\right]^{1/2} \sum_{n=-k}^{k} Y_{k,n}^*(\varepsilon_2, \varepsilon_1) \\ &\times \sum_{n'=-k}^{k} Y_{k,n'}^*(\omega_j) R_{k,n',n}(\alpha, \beta, \gamma) \\ &\times j_l(Qr_j) \sum_{m'=-l}^{l} R_{l,m',m}(\alpha, \beta, \gamma) Y_{l,m'}^*(\omega_j). \end{aligned} \quad (36)$$

The product of the matrix elements of the rotation operator can be contracted to a sum of these. Using (47), one obtains

$$\begin{aligned} B_{l,m}(Q, \alpha, \beta, \gamma, \varepsilon) &= (i)^l \sum_j \sum_{k=0,2,4} C_k \left[\frac{4\pi}{2k+1}\right]^{1/2} \\ &\times \sum_{n=-k}^{k} Y_{k,n}^*(\varepsilon_2, \varepsilon_1) \sum_{n'=-k}^{k} Y_{k,n'}^*(\omega_j) j_l(Qr_j) \\ &\times \sum_{m'=-l}^{l} Y_{l,m'}^*(\omega_j) \sum_{\eta=|l-k|}^{l+k} (2\eta+1) \begin{pmatrix} l & k & \eta \\ m' & n' & p \end{pmatrix} \\ &\times \begin{pmatrix} l & k & \eta \\ m & n & q \end{pmatrix} R_{\eta,p,q}(\alpha, \beta, \gamma). \end{aligned} \quad (37)$$

The intensity of scattering from randomly oriented particles is obtained by integration over α, β, γ. Introducing (37) in (12), the equation contains the orthogonality relation of the matrix elements of the rotation operator (46).

$$\frac{1}{8\pi^2} \int_{\alpha=0}^{2\pi} \int_{\beta=0}^{\pi} \int_{\gamma=0}^{2\pi} R_{\eta_1,p_1,q_1}(\alpha, \beta, \gamma) R_{\eta_2,p_2,q_2}^*(\alpha, \beta, \gamma) \, \mathrm{d}\alpha \sin\beta \, \mathrm{d}\beta \, \mathrm{d}\gamma = \frac{1}{2\eta+1} \delta_{\eta_1,\eta_2} \delta_{p_1,p_2} \delta_{q_1,q_2}, \quad (38)$$

which requires that $\eta_1 = \eta_2$, $p_1 = p_2$ and $q_1 = q_2$. The average scattering intensity from close protons as parts of randomly oriented particles subjected to the angular part of (1) is

$$\begin{aligned} I_{BB}(\mathbf{Q}, \varepsilon) &= \sum_{l_1=0}^{\infty} \sum_{l_2=0}^{\infty} i^{l_1} (-i)^{l_2} \sum_{l=|l_1-l_2|}^{l_1+l_2} \sum_{m=-l}^{l} \sum_{m_1=-l_1}^{l_1} \sum_{m_2=-l_2}^{l_2} (-1)^{m+m_2} \\ &\times \left[\frac{(2l_1+1)(2l_2+1)(2l+1)}{4\pi}\right]^{1/2} \begin{pmatrix} l_1 & l_2 & l \\ m_1 & -m_2 & m \end{pmatrix} \\ &\times \begin{pmatrix} l_1 & l_2 & l \\ 0 & 0 & 0 \end{pmatrix} \sum_{k_1=0,2,4} \sum_{k_2=0,2,4} \frac{4\pi C_{k_1} C_{k_2}}{[(2k_1+1)(2k_2+1)]^{1/2}} \\ &\times \sum_{n_1=-k_1}^{k_1} \sum_{n_2=-k_2}^{k_2} Y_{k_1,n_1}^*(\varepsilon_2, \varepsilon_1) Y_{k_2,n_2}(\varepsilon_2, \varepsilon_1) \sum_{\eta} (2\eta+1) \\ &\times \sum_{n_1'=-k_1}^{k_1} \sum_{n_2'=-k_2}^{k_2} \sum_{m_1'=-l_1}^{l_1} \sum_{m_2'=-l_2}^{l_2} \begin{pmatrix} l_1 & k_1 & \eta \\ m_1' & n_1' & p \end{pmatrix} \begin{pmatrix} l_1 & k_1 & \eta \\ m_1 & n_1 & q \end{pmatrix} \\ &\times \begin{pmatrix} l_2 & k_2 & \eta \\ m_2' & n_2' & p \end{pmatrix} \begin{pmatrix} l_2 & k_2 & \eta \\ m_2 & n_2 & q \end{pmatrix} \\ &\times \sum_{j_1} \sum_{j_2} Y_{k_1,n_1'}^*(\omega_{j_1}) Y_{k_2,n_2}(\omega_{j_2}) \\ &\times j_{l_1}(Qr_{j_1}) j_{l_2}(Qr_{j_2}) Y_{l_1,m_1'}^*(\omega_{j_1}) Y_{l_2,m_2'}(\omega_{j_2}) Y_{l,-m}(\Omega). \end{aligned} \quad (39)$$

For η two conditions hold: $|l_1 - k_1| \le \eta \le l_1 + k_1$ and $|l_2 - k_2| \le \eta \le l_2 + k_2$.

APPENDIX C

The following formulae have been used. They can be found for example in textbooks of electrodynamics or quantum mechanics and they are given here for the convenience of the reader.

$$\exp(i\mathbf{Q} \times \mathbf{r}) = 4\pi \sum_{l=0}^{\infty} \sum_{m=-l}^{l} i^l j_l(Qr) Y_{l,m}^*(\omega) Y_{l,m}(\Omega). \quad (40)$$

j_l are the spherical Bessel functions. The spherical harmonics $Y_{l,m}$ form a complete orthogonal set on the surface of a unit sphere in the two indices l, m. $\omega(\theta, \varphi)$ and $\Omega(\Theta, \phi)$ are unit vectors in $\mathbf{r}$ and $\mathbf{Q}$ space, respectively.

$$\int_0^{2\pi} \mathrm{d}\varphi \int_0^{\pi} \sin\theta \, \mathrm{d}\theta \, Y_{l',m'}^*(\theta, \varphi) Y_{l,m}(\theta, \varphi) = \delta_{l',l} \delta_{m',m}. \quad (41)$$

For negative indices m, the following holds:

$$Y_{l,-m}(\omega) = (-1)^m Y_{l,m}^*(\omega). \quad (42)$$

The product of spherical harmonics can be reduced to a sum of these (rule of contraction):

$$\begin{aligned} Y_{l_1,m_1}(\omega) Y_{l_2,m_2}(\omega) &= \sum_{l=|l_1-l_2|}^{l_1+l_2} \sum_{m=-l}^{l} (-1)^m \left(\frac{(2l_1+1)(2l_2+1)(2l+1)}{4\pi}\right)^{1/2} \\ &\times \begin{pmatrix} l_1 & l_2 & l \\ 0 & 0 & 0 \end{pmatrix} \begin{pmatrix} l_1 & l_2 & l \\ m_1 & m_2 & m \end{pmatrix} Y_{l,-m}(\omega). \end{aligned} \quad (43)$$

For the Wigner $3j$ symbols in brackets $(\ldots)$, the following holds: $m_1 + m_2 = m$. If $m_1 = 0$ and if $m_2 = 0$, then the value of the $3j$ symbol will vanish unless $l_1 + l_2 + l$ is even.

The formula for the rotation of spherical harmonics by the Eulerian angles (α, β, γ) is

$$Y_{l,m}(\omega') = \sum_{m'=-l}^{l} R_{l,m',m}(\alpha, \beta, \gamma) Y_{l,m'}(\omega), \tag{44}$$

where $R_{l,m',m}(\alpha, \beta, \gamma)$ are the matrix elements of the rotation operator. In particular, for $m = 0$,

$$R_{l,m,0}(\alpha, \beta, 0) = \left(\frac{4\pi}{2l+1}\right)^{1/2} Y^*_{l,m}(\beta, \alpha). \tag{45}$$

The orthogonality of the matrix elements of the rotation operator requires

$$\frac{1}{8\pi^2} \int_{\alpha=0}^{2\pi} \int_{\beta=0}^{\pi} \int_{\gamma=0}^{2\pi} \mathrm{d}\alpha \sin\beta \, \mathrm{d}\beta \, \mathrm{d}\gamma \, R_{l_1,m_1,n}(\alpha, \beta, \gamma) R^*_{l_2,m_2,n_2}(\alpha, \beta, \gamma)$$
$$= \frac{1}{2l_1+1} \delta_{l_1,l_2} \delta_{m_1,m_2} \delta_{n_1,n_2}. \tag{46}$$

The product of the matrix elements of the rotation operator can be contracted to a sum of these:

$$R_{l_1,m_1,n_1}(\alpha, \beta, \gamma) R_{l_2,m_2,n_2}(\alpha, \beta, \gamma)$$
$$= \sum_{l=|l_1-l_2|}^{l_1+l_2} (2l+1) \begin{pmatrix} l_1 & l_2 & l \\ m_1 & m_2 & m \end{pmatrix} \begin{pmatrix} l_1 & l_2 & l \\ n_1 & n_2 & n \end{pmatrix}$$
$$\times R_{l,m,n}(\alpha, \beta, \gamma). \tag{47}$$

The experiments on polarized neutron scattering from dynamically polarized proton spin targets were carried out at the instrument D22 of the Institut Laue–Langevin, Grenoble, France, using the polarized target facility of PSI, Villigen, Switzerland. The author is indebted to Ben van den Brandt, Patrick Hautle, Ton Konter, Joachim Kohlbrecher and Salvatore Mango from PSI, Villigen, Switzerland, Hans Glättli (CEA/LLB, Saclay, France), Edouard Leymarie (CNRS, Villefranche, France), Roland May, Isabel Grillo and Oliver Zimmer from ILL, Grenoble, France, who as a team made the experiments possible. The author would also like to thank Hans Glättli and Tapio Niinikoski (CERN, Geneva, Switzerland) for their helpful comments on this paper.

References

Abragam, A. & Goldman, M. (1978). *Rep. Prog. Phys.* **41**, 395–467.
Abragam, A. & Goldman, M. (1982). *Nuclear Magnetism: Order and Disorder.* Oxford: Clarendon Press.
Brandt, B. van den, Glättli, H., Grillo, I., Hautle, P., Jouve, H., Kohlbrecher, J., Konter, J. A., Leymarie, E., Mango, S., May, R. P., Michels, A., Stuhrmann, H. B. & Zimmer, O. (2006). *Eur. Phys. J.* B**49**, 157–165.
Brandt, B. van den, Glättli, H., Grillo, I., Hautle, P., Jouve, H., Kohlbrecher, J., Konter, J. A., Leymarie, E., Mango, S., May, R. P., Stuhrmann, H. B. & Zimmer, O. (2002). *Europhys. Lett.* **59**, 62–67.
Brandt, B. van den, Glättli, H., Grillo, I., Hautle, P., Jouve, H., Kohlbrecher, J., Konter, J. A., Leymarie, E., Mango, S., May, R. P., Stuhrmann, H. B. & Zimmer, O. (2003). *Physica (Utrecht)*, B**335**, 193–195.
Cox, S. F. J. (1980). Proceedings of the Second Workshop on Polarized Target Materials, edited by G. R. Court, S. F. J. Cox, D. A. Cragg & T. O. Niinikoski. Report RL-80-080, p. 74, Rutherford Appleton Laboratories, Didcot, UK.
Cox, S. F. J., Read, S. F. J. & Wenckebach, W. Th. (1977). *J. Phys. C*, **10**, 2917–2936.
Finch, J. T. & Holmes, K. C. (1967). *Methods in Virology*, edited by K. Maramorosch & H. Koprowski, Vol. 3, pp. 351–474. New York: Academic Press.
Hayter, J. B., Jenkin, G. T. & White, J. W. (1974). *Phys. Rev. Lett.* **33**, 696–699.
Krumpolc, M. & Rožek, J. (1979). *J. Am. Chem. Soc.* **101**, 3206–3209.
Niinikoski, T. O. (1980). Proceedings of the Second Workshop on Polarized Target Materials, edited by G. R. Court, S. F. J. Cox, D. A. Cragg & T. O. Niinikoski. Report RL-80-080, pp. 60–65, Rutherford Appleton Laboratories, Didcot, UK.
Stuhrmann, H. B. (1970). *Acta Cryst.* A**26**, 297–306.
Wenckebach, W. Th. (1980). Proceedings of the Second Workshop on Polarized Target Materials, edited by G. R. Court, S. F. J. Cox, D. A. Cragg & T. O. Niinikoski. Report RL-80-080, p. 73, Rutherford Appleton Laboratories, Didcot, UK.